Quantum oscillations in hcp Co_2/Si_n superlattice related to lattice symmetry

Jijun Xue, Leikai Ma, and Hua Pang*
Institute of Applied Magnetics, Key Laboratory For Magnetism and Magnetic Materials of the Ministry of Education, Lanzhou University, Lanzhou 730000, China

(Received 15 June 2022; accepted 10 July 2023; published 31 July 2023)

Heterostructures composed of different elements are a suitable platform for many novel physical phenomena. Here, quantum oscillations related to the lattice symmetry in hexagonal close-packed (hcp) Co_2/Si_n superlattices, such as lattice parameters, electronic structure, and magnetism, are revealed and studied by density-functional theory. Densely packed atomic layers stack in an *ABAB* sequence in the superlattice and reach a bilayer-like structure by interlayer coupling in the presence of the Co/Si interface. The lattice symmetry depends on the parity of n, and an odd number of n benefits interlayer coupling and the interface effect, causing odd-even quantum oscillations. These observations indicate that changing lattice symmetry by designing component type, layer number, and stacking sequence is a feasible method of effectively regulating the performance of ultrathin heterojunctions.

DOI: 10.1103/PhysRevB.108.035426

I. INTRODUCTION

Metal-semiconductor superlattices have attracted extensive attention recently. One motivating factor is that compared with their bulk counterparts, the superlattices may exhibit novel and exotic structural and electronic properties [1–5], such as artificial symmetry breaking of heterojunctions, electron confinement in metal layers, mid-to-long-wavelength phonons, hyperbolic photonic dispersion under the transverse magnetic wave, etc. Therefore, they have potential applications in electronic, optoelectronic, thermal transport, and commercial terahertz devices. More importantly, there are also some atomic-scale effects due to atomic-scale manipulation of the materials. A prominent example is the oscillations of various physical properties concerning the thickness of the atomic layers. For many lattice-matched systems, the oscillation periods are predicted to be the spanning vectors of the spacer-layer Fermi surface theoretically and evidenced experimentally, which typically correspond to the thickness of several monolayers [6,7]. In recent years, short-period oscillations of physical properties such as band gap, friction, work function, and diffusion barrier have been reported in some heterostructures and two-dimensional materials [8–11], as well as odd-even oscillations in exchange coupling in systems such as Co/Si, Co/C, Cr/C, and $L1_0$−Mn Ga/Co [12–15]. The interlayer coupling has a significant effect on these oscillations, and the coupling mechanism deserves further study.

Various approaches, such as chemical composition [14], film thickness [9], and the local environment [8] of the magnetic atoms, have been successfully used to modulate interlayer interaction. Since interlayer coupling is closely associated with crystal symmetry, the lattice structure provides another available freedom. Due to the development of artificial multilayer techniques, such as molecular-beam epitaxy [16–19], it is possible to adjust the lattice symmetry, for example, by properly designing the chemical composition, growth sequence, and the number of layers on either side of the interface. In this regard, multilayers with the hexagonal close-packed (hcp) structure have advantages because the closely packed atomic monolayers stack in an *ABAB* sequence in an hcp crystal, and thereupon multilayer structures with and without complete *AB* periods naturally have different space groups. For example, the space group is $P-3m1$ for an isolated hcp Co multilayer with an even number of Co layers, while it is $P-6m2$ for the one with an odd number. Compared with chemical means like element doping, it is a more macroscopic perspective to tailor the material properties by tuning the symmetry of the metal-semiconductor heterostructures, and worth further investigation.

This work presents a detailed study of the electronic and magnetic properties of hcp Co_2/Si_n superlattice, an alternant structure of two Co layers and n layers of Si, using first-principles calculations. The bulk Co is an hcp-structured metal with itinerate magnetism, and bulk hcp-Si is stable and metallic at high pressure [20]. We chose this system to study short-period quantum oscillation for two reasons. First, hcp Co_2/Si_n superlattice is a magnetic metal and exhibits rich physical phenomena. Second, strong interaction between Co and Si atomic layers is requisite for forming the Co/Si interface and quantum oscillation. In the present work, we focus on the influence of lattice symmetry on the electronic properties and ignore the Co-Si amorphous layer observed in experiments [21,22]. The global symmetry of the hcp Co_2/Si_n superlattice varies with the parity of n, and the superlattice reaches a bilayer-like structure due to the combined interaction of the bilayer stacking periodicity of the hcp lattice and the interface potential, resulting in the odd-even oscillations of the lattice parameters, the magnetic ground states, the magnetic moments of Co atoms, and the band splitting due to spin-orbit coupling (SOC), etc.

*hpang@lzu.edu.cn

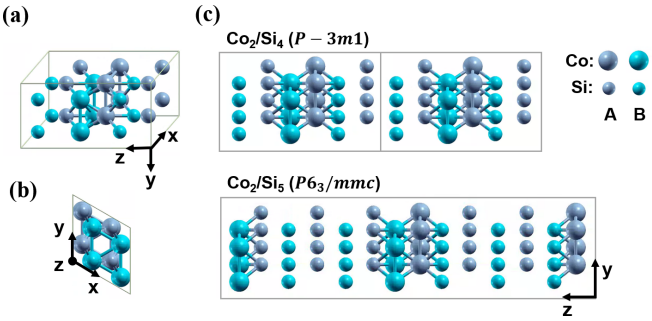

FIG. 1. (a) Unit cell of hcp Co_2/Si_4 superlattice. Side view of XY plane is shown in (b). (c) Two unit cells of hcp Co_2/Si_4 (upper panel) and one unit cell of hcp Co_2/Si_5 (bottom panel), for which space groups are $P-3m1$ and $P6_3/mmc$, respectively. Big balls represent Co atoms, small balls represent Si atoms, gray balls represent A layer, and blue balls represent B layer.

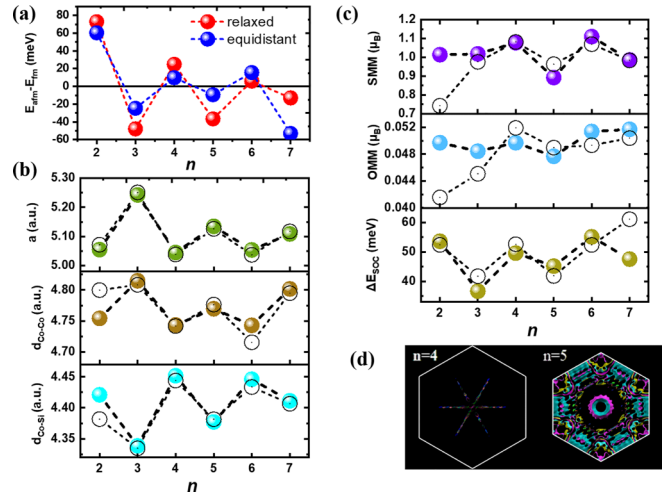

FIG. 2. (a) Energy difference between ferromagnetic (FM) state and antiferromagnetic (AFM) state vs n for fully relaxed hcp Co_2/Si_n superlattices and equal interlayer spacing. (b) Evolutions of lattice parameters a, interlayer distance of Co_2, and that between neighboring Co and Si layers with n. (c) Spin magnetic moment (SMM), orbital magnetic moment (OMM), and energy splitting ΔE_{soc} due to spin-orbit coupling (defined in text) vs n. Solid spheres represent FM coupling, and hollow spheres represent AFM coupling in (b) and (c), where dotted lines are a guide to the eye. (d) Fermi-surface structure for $n = 4$ and 5 cases at FM state.

II. METHODS

To set up an hcp Co_2/Si_n superlattice, each Co or Si atomic single layer was close-packed plane and stacked in an $ABAB$ sequence with every Si_n layer (n from 1 to 7) followed by a Co_2 layer. In this way, the c axis of the superlattice was parallel to the z axis of the supercell [Fig. 1(a)]. The layer spacing and in-plane atomic distance were the corresponding values of bulk hcp Co initially [23]. Then, the atomic coordinates and the lattice constants were fully relaxed using the conjugate-gradient algorithm until the maximum force on each atom was less than 1.0 mRy/Å.

All calculations were performed using the WIEN2K package [24,25]. The full-potential linearized augmented plane-wave method was adopted, and the generalized gradient approximation (Perdew-Burke-Wang form) was employed for the exchange-correlation potential. The radii of muffin-tin (MT) spheres of Co and Si atoms were set as 2.20 and 2.06 a.u., respectively. The potential and the charge density in the MT spheres were expanded in the spherical harmonics with $l_{max} = 10.0$. The convergence of the total energy difference of the system when magnetized along the (1000) and (0001) directions after including SOC was used to determine the values of the calculated parameters, with an energy criterion of 0.2 meV/f.u. The plane-wave cutoff parameter ($R_{MT} \times K_{max}$) was 7.0, and the magnitude of the largest vector G_{max} was 14.0. The Monkhorst-Pack k-point meshes for the irreducible Brillouin zone were $38 \times 38 \times 7$, $38 \times 38 \times 5$, $37 \times 37 \times 3$, and $37 \times 37 \times 2$ when $n = 1$, 3, 5, and 7, respectively, while the grids were $32 \times 32 \times 9$, $34 \times 34 \times 6$, and $34 \times 34 \times 5$ when $n = 2$, 4, and 6.

III. RESULTS AND DISCUSSION

The parity of n results in different crystal symmetry for the hcp Co_2/Si_n primitive cell. As shown in Fig. 1(c), when n is even, the AB stacking sequence along the c axis in adjacent Co_2 layers is the same, while the AB sequence is opposite for the adjacent Co_2 layers when n is odd. Therefore, there is only one Co_2 layer in the unit cell when n is even, and the crystals belong to space group $P-3m1$ (No. 164); see hcp Co_2/Si_4 in Fig. 1(c). The unit cell includes two Co_2 layers when n is odd, leading to a $P6_3/mmc$ (No. 194) space group, like hcp Co_2/Si_5 in Fig. 1(c).

As shown in Fig. 1, many properties of hcp Co_2/Si_n oscillate with the parity of n. First, consistent with previous reports [12,13], the interlayer exchange coupling between adjacent Co_2 layers separated by n layers of Si manifests as odd-even quantum oscillation with a period of two Si layers for systems with fully relaxed structures [red balls in Fig. 2(a)] and with equal interlayer spacing [blue balls in Fig. 2(a)], i.e., it is antiferromagnetic (AFM) coupling when n is odd and ferromagnetic (FM) coupling when n is even.

Second, the lattice parameters of fully relaxed hcp Co_2/Si_n superlattice exhibits odd-even oscillation independent of exchange coupling [Fig. 2(b), where solid spheres correspond to FM coupling and hollow spheres correspond to AFM coupling]. According to our calculations, the lattice parameters for bulk hcp Co was $a = 4.70$ a.u. with an a/c ratio of 0.62, and the distance between the two nearest-neighboring Co atoms from adjacent layers along the c axis is $d_{Co-Co} = 4.68$ a.u., consistent with the literature [23]. Compared to bulk hcp Co, the unit cell of hcp Co_2/Si_n expands along the c axis and the ab plane, yielding a slightly larger a/c ratio. Taking FM-coupled hcp Co_2/Si_5 as an example, $a = 5.14$ a.u., $a/c = 0.67$, $d_{Co-Co} = 4.76$ a.u., and the atomic spacing of the Co-Si interface is $d_{Co-Si} = 4.36$ a.u., the shortest of all interatomic distances, a signature of interface effect. With the change in the number of Si layers, all lattice parameters exhibit the law of odd-even oscillation. Specifically, a and d_{Co-Co} are larger when n is odd, while c and d_{Co-Si} are larger when n is even.

Third, except for hcp Co_2/Si_2, the magnetic moments of Co atoms in the hcp Co_2/Si_n superlattices show the law of

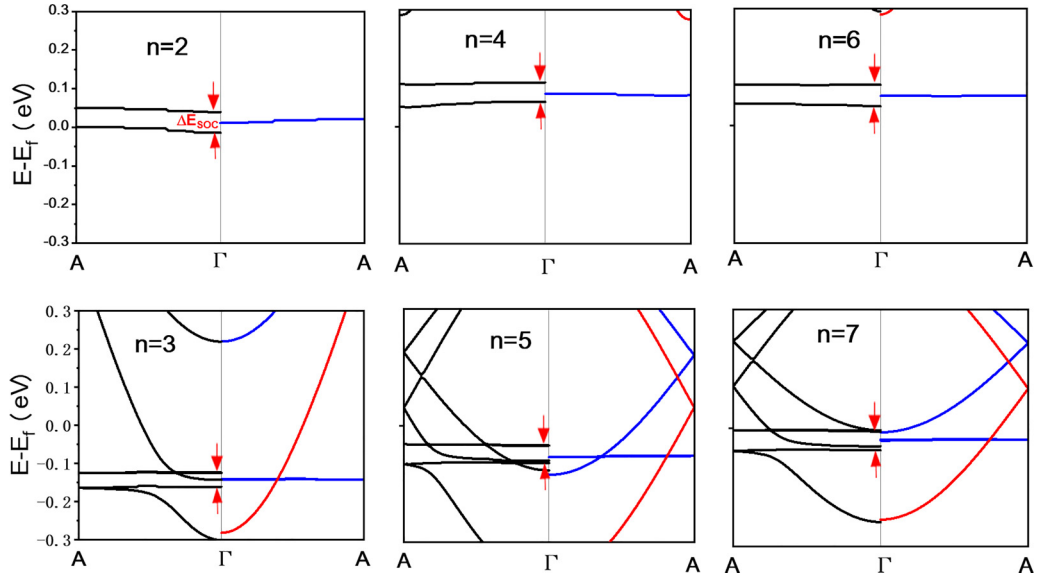

FIG. 3. Band diagram along k_z direction near E_f for FM-coupled Co_2/Si_n structures. Right half of each figure is case without SOC, where spin-majority band and spin-minority band are red and blue lines, respectively. Left half is case with SOC, where SOC-induced band splitting is marked by red arrows.

odd-even oscillation, both for FM and AFM coupling [Fig. 2(c)], where FM coupling is denoted by solid spheres and AFM coupling by hollow spheres). The spin magnetic moment (SMM) and orbital magnetic moments (OMM) are enhanced when n is odd and reduced when n is even. The anomaly of hcp Co_2/Si_2 can be ascribed to its stronger FM coupling than other systems due to the smaller spacing between adjacent Co_2 layers. It is worth noting that Co induces spin polarization of its neighbor Si atoms, which decay rapidly with distance. For example, in hcp Co_2/Si_5, the magnetic moment of the first-nearest-neighbor Si atom is 0.021 μ_B, and the next-nearest neighbor is 0.0015 μ_B.

Another crucial property in magnetic materials is spin-orbit coupling. To quantitatively describe the strength of SOC effects in hcp Co_2/Si_n superlattice, we examine bands near the Fermi level along the k_z direction (from Γ to A), which presents in all systems regardless of the parity of n. This band is flat in the absence of SOC (right panels in Fig. 3) and splits into two after turning on SOC (left panels in Fig. 3), which makes it practicable to evaluate the n dependence of the SOC effect. In addition, there are two other advantages to this choice. First, in the absence of SOC, the exchange splitting between the spin-majority states and the spin-minority states is about 1.0 eV; hence, the mixing of the two spin states after including SOC is insignificant. Second, no other band lies closely around the Γ point and only a few energy bands intersect along the given path. So, the SOC-related phenomena, such as band crossing or anticrossing, are far away from the Γ point. The SOC splitting, evaluated by the band splitting ΔE_{SOC} at the Γ point, is an order of magnitude larger than that in bulk cobalt [26] and shows an odd-even quantum oscillation with n [Fig. 2(b)], i.e., it peaks when n is even and troughs when n is odd. The enhancement of SOC splitting in hcp Co_2/Si_n compared to bulk Co can be due to the electrons confined in the metallic layers, which experience an electric field from a Dresselhaus term caused by bulk-inversion asymmetry and a Rashba term due to structure-inversion asymmetry at the interface [27–29], favoring large SOC.

Finally, the electronic structures near the Fermi energy (E_f) present odd-even quantum oscillations in the hcp Co_2/Si_n superlattice. Figure 4 plots the density of states (DOS) of Co-d (blue) and Si-p (red) for FM (solid line)- and AFM (dashed line)-coupled hcp Co_2/Si_n supercells. Except for hcp Co_2/Si_2, the features of the DOSs are similar around E_f for the two coupling cases of each system, and the anomaly of hcp Co_2/Si_2 can be due to its more enhanced FM coupling than other systems. The DOS around E_f is dominated by spin-minority states of Co-3d electrons for each system, while the spin-majority Co-3d states are occupied. Interestingly, although the contour details vary with n, the DOS peak position varies with the parity of n, i.e., it is below E_f when n is odd, while it is just above E_f when n is even. Figure 3 also demonstrates that the band structure near E_f varies with the parity of n for the hcp Co_2/Si_n superlattice. When n is even, the flat band lies above E_f, and the Fermi level locates in a pseudogap. When n is odd, the flat bands are below E_f, and the Fermi level passes through several bands, indicating metallic property and a large Fermi surface. Figure 2(d) shows the Fermi surface of FM-coupled hcp Co_2/Si_n in the first Brillouin zone when $n = 4$ and $n = 5$. The Fermi surface for $n = 4$ is small and contains three intersecting planes, for which the angle between each plane is 120°. The shape and approximately two-dimensional properties are similar to the isolated hcp Co_2 slab, coinciding with the fewer bands passing through E_f, while for $n = 5$ all five 3d orbitals pass through E_f, resulting in a complex three-dimensional Fermi surface. One may expect that the properties related to the Fermi surface, such as heat conduction and optical properties, will also show oscillation behaviors associated with the parity of n.

It seems the odd-even quantum oscillations in the lattice structure, electronic structure, and magnetic properties are

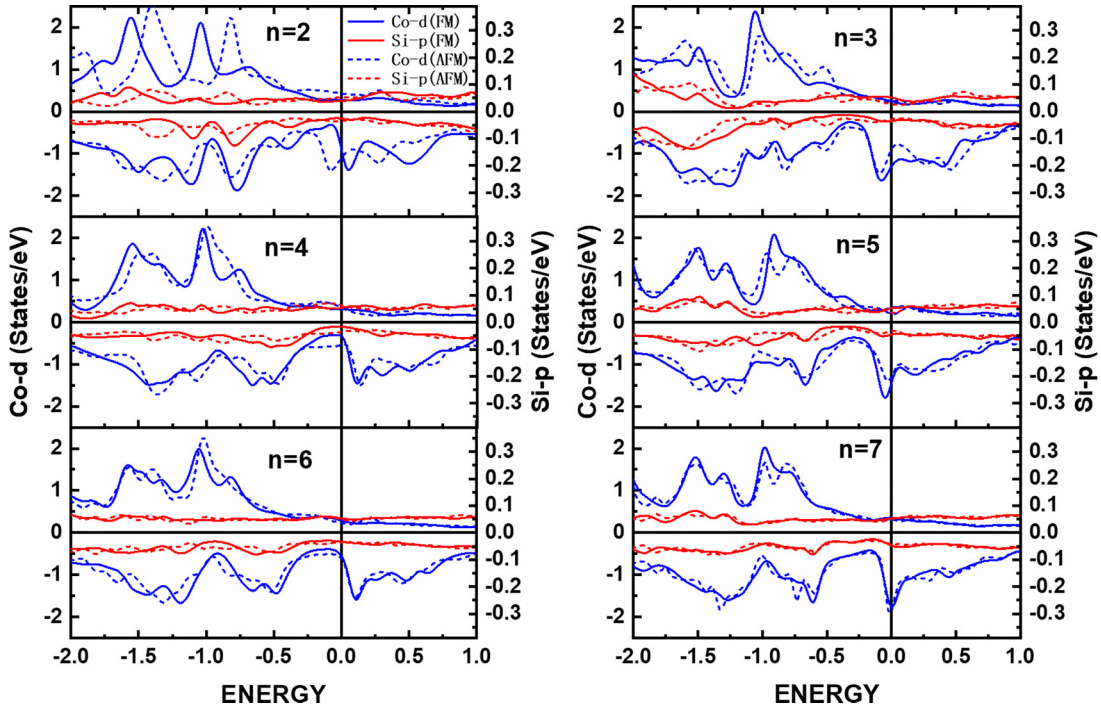

FIG. 4. Density of states of Co-3*d* electrons (in blue) and Si-2*p* electrons (in red) of hcp Co_2/Si_n superlattice with FM coupling (solid lines) and AFM coupling (dotted lines) around Fermi energy. Positive and negative values of energy indicate spin-majority state and spin-minority state, respectively.

independent of the exchange coupling but depend on the lattice and orbital freedoms of hcp Co_2/Si_n, which are closely related to the symmetry of the superlattice. Moreover, the parity oscillation of exchange coupling is preserved for systems with equal layer spacing, which further excludes the causal relationship between exchange coupling and other properties. Then, we will focus on the case of FM coupling below.

The heterostructure of hcp Co_2/Si_n can be regarded as the combination of double-layer Co and n-layer Si. To understand the cause of observed oscillations, we turn to the isolated hcp Si_n. Experimentally hcp Si_n is stable and metallic at high pressure [20,30,31]. For example, when the pressure is 42.5 GPa, the lattice constant a of hcp Si_n is 4.67 a.u. with the a/c ratio of 0.59. When establishing the isolated hcp Si_n model systems, the initial spacing between the close-packed Si layers was equal and set to 4.70 a.u., while the lattice constant a was set as that of the optimized hcp Co_2/Si_n supercells. The center position of Si_n was at $z = 0.5$, and the spacing between the surface Si layer to the top or bottom of the unit cell was more than 35 Å to meet the conditions of an isolated slice.

After full structural optimization, the Si_n slab tends to form a bilayer-like structure. For convenience, we mark the bottom surface of the slab as layer A_1, the layer immediately above it as layer B_1, then comes A_2, B_2, and so on (Fig. 5). The slab terminates on layer $B_{n/2}$ (the upper surface) when n is even and ends on layer $A_{(n+1)/2}$ when n is odd. When n is even, starting from the surface layers and moving inward, the interlayer spacing d_i between the adjacent A_i and B_i layers (i denotes the sequence of the atomic layer) increases while the spacing D_i between two adjacent B_i and A_{i+1} layers decreases. Note that the value of D_i is always larger than d_i, indicating that the adjacent A_i and B_i layers tend to approach each other starting from the surface, forming an A_i-B_i bilayer structure. For example, when $n = 4$, d_1 (the spacing between A_1 and B_1 layers) $= d_2$ (the spacing between A_2 and B_2 layers) $=$ 4.20 a.u. and the interlayer distance between the two bilayers is $D_1 = 2.33$ Å. When n is odd it is a little more complicated, but the tendency to form the bilayer-like structure is the same. Still, the distance within bilayers is referred to as d_i, and the distance between bilayers is D_i. Take Si_5 as an example.

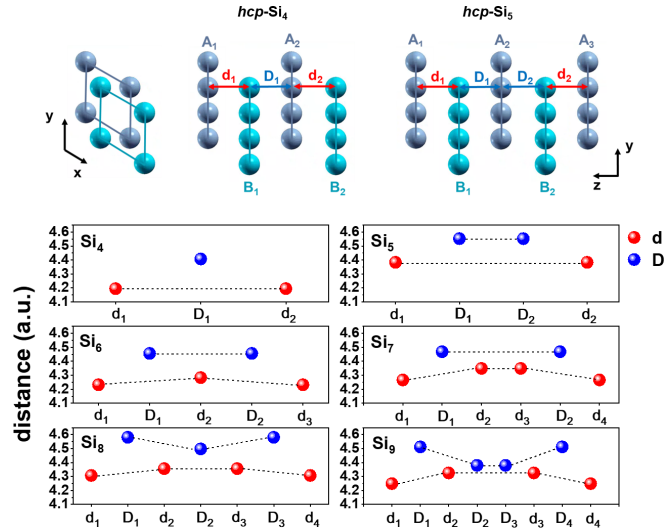

FIG. 5. Schematic illustration of spacing d_i between adjacent A_i and B_i layers and interlayer distance D_i between two AB bilayers (top panel), and distribution of d_i and D_i along c axis in isolated hcp Si_n (bottom panel). Dotted lines are guides to the eye.

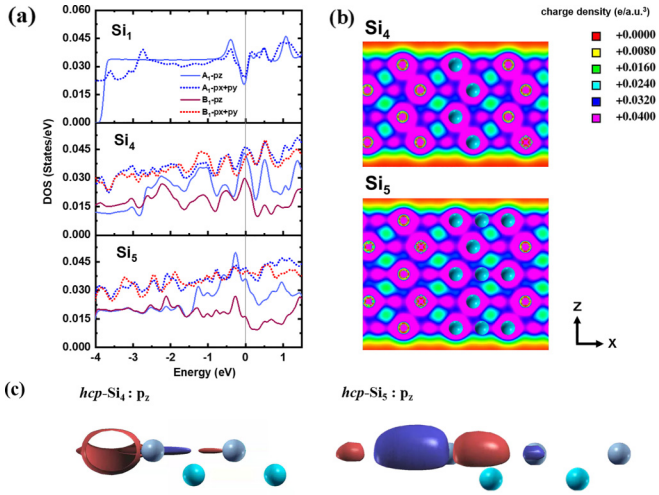

FIG. 6. (a) Density of states (DOS) of Si_n. (b) Valence charge density in xz plane of Si_4 and Si_5. (c) Wannier functions of p_z orbitals for outermost Si atoms in isolated hcp Si_4 and hcp Si_5.

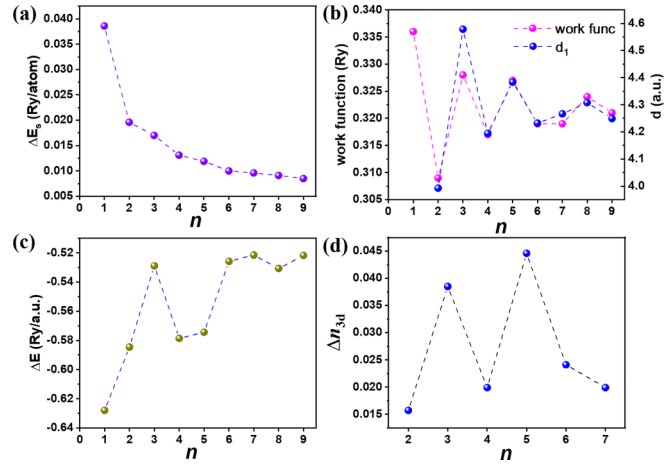

FIG. 7. Surface energy ΔE_s (a); interlayer distance d_1 and work function (b) of isolated hcp Si_n. Formation energy ΔE (c) and increase in Co-3d occupation number (d) after formation of Co-Si interface for Co_2/Si_n heterostructures. Dotted line in figure represents trend of change of points as n increases.

The two surface layers (A_1 and A_3) form bilayers (A_1-B_1 and B_2-A_3) with $d_1 = d_2 = 4.40$ a.u. The third layer in the middle, namely A_2, is equally spaced with the two bilayers with a distance of $D_1 = D_2 = 5.39$ a.u. In general, the closer the A-B bilayer is to the surface, the smaller the inner spacing is.

The emergence of a bilayer-like structure in isolated hcp-Si_n comes from the surface-effect modulated electronic interlayer coupling. The valence electron configuration of silicon is $3s^2\,3p^2$, which is the most favorable to a diamond structure where each Si atom forms covalent bonds with the other four Si atoms with sp^3 hybrid orbitals, and the nearest Si-Si atom spacing is 2.35 Å. In silicene monolayer, the atomic spacing is about 2.40 Å, which weakens π electron overlapping compared with graphene and results in a honeycomb structure folded along the z direction by a mixture of sp^2 and sp^3 hybridization. In the hcp-Si_n multilayer, Si atoms belonging to the same layer form a triangular lattice, just like putting an extra Si atom at the honeycomb center of silicene, which further increases the in-plane atomic spacing to save Coulomb energy. The spacing between Si atoms in the same layer is about 2.70 Å. Now, the nearest neighbor of a Si atom is not from the same close-packed layer but from the adjacent layer above and below. Although this destroys the possibility of forming various s-p hybrid orbitals, it is favorable for interlayer electron interactions. The electronic structures provide support. Compared with Si_1, a two-dimensional case, the calculated density of states have more complex structures near E_f for Si_n with a larger n. Take the surface bilayer A_1-B_1 in Si_4 and Si_5 for examples. For the two systems, the DOSs of p_z electrons in layer A_1 and layer B_1 have similar contours around E_f [solid lines in Fig. 6(a)], which fully indicates the existence of p-p interaction between the two layers. The valence charge density in the xz plane affords further support [Fig. 6(b)]. The non-negligible electron density between surface layer A and its adjacent layer B undoubtedly evidences chemical bonding between the two layers, while the charge density between the two bilayers is relatively low.

One quantity in characterizing a surface is surface energy. Considering that the hcp Si_n slab has nonpolar surfaces, the surface energy can be expressed as the energy difference between bulk hcp Si and the slab. Here, the surface energy per Si atom is described as $\Delta E_s = (E_{\text{bulk}}/2) - (E_{\text{slab}}/n)$, where E_{bulk} represents the energy of an hcp Si bulk. The calculation results [Fig. 7(a)] show that the ΔE_s decreases monotonically with the increase of n and tends to be constant when n exceeds 6, indicating a relatively long-range surface effect of Si_n. The local environment of Si atoms in the surface layer is highly asymmetric along the c axis, with a vacuum on one side and a crystalline field on the other, which is conducive to the covalent bonding between the surface atom and its inner neighbor to form an A-B bilayer. As a result, the interlayer spacing reduces for the bilayer, and the crystalline field experienced by the third layer becomes asymmetrical, inducing covalent interaction between the third and fourth layers. This effect propagates from the surface to the center, eventually resulting in an A-B bilayer-like structure.

It turns out that the interlayer coupling strength is strongly related to the parity of n, which decides the lattice symmetries of hcp Si_n. Due to the AB stacking periodicity of hcp crystals, the point group is $P\bar{3}m1$ ($P\bar{6}m2$) when n is even (odd) for isolated hcp Si_n. The slab with odd n has a mirror symmetry with the middle layer as the reflection mirror. When counting A-B bilayers from the outside to the inside, the number of A-B bilayers is an integer when n is even, while the mirror layer is redundant in the case of odd n. The incommensurate in the latter case acts as a disturbance when forming the bilayer structures, which weakens the interlayer coupling of the bilayers. As shown in Fig. 6(a), when n is odd, such as hcp-Si_5, the density peak of p_z electrons lies below E_f. When n is even, such as hcp Si_4, the Fermi level runs through the center of p_z electron density, demonstrating relatively strong interlayer coupling. The Wannier function [32,33] of the Si-p_z electrons at the surface layer further proves this [Fig. 6(c)]. Compared to the case of hcp Si_4, the p_z orbital of hcp Si_5 is more like the situation in an isolated atom, a signature of

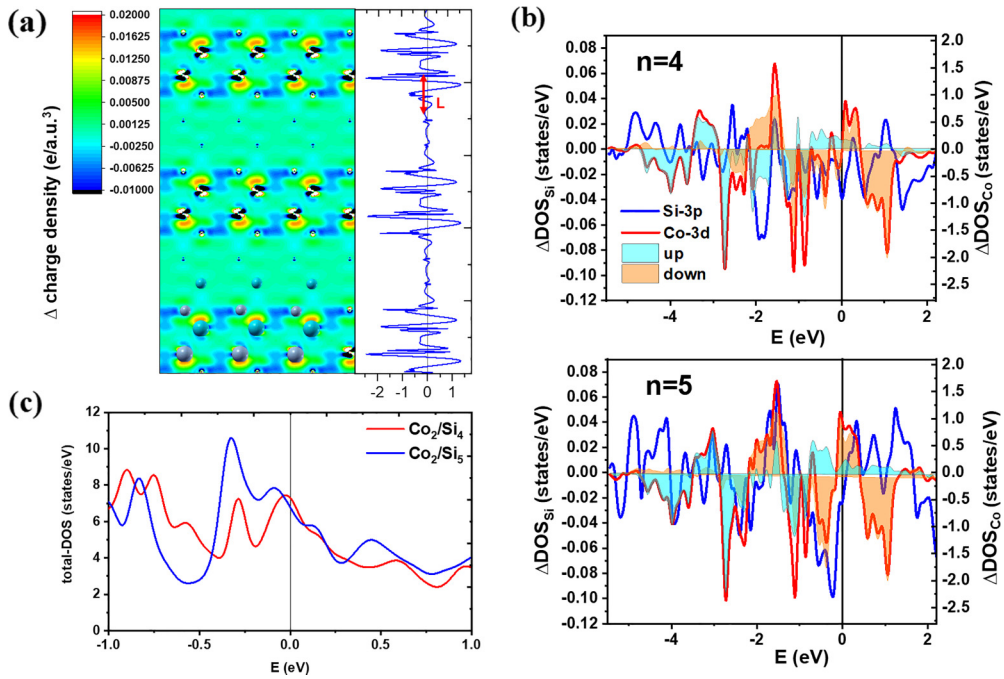

FIG. 8. (a) Difference in electron density distribution before and after interface formation for Co_2/Si_4 (left panel) and profile of density difference along z direction of supercell (right panel), where red arrow indicates electron redistribution interval L. (b) Difference in DOS before and after formation of Co-Si interface (ΔDOS) for Co_2/Si_n ($n = 4$ and 5). Orange (blue) shadows denote redistribution of spin-minority (-majority) Co-3d states, which explains odd-even oscillations of magnetic moment. (c) DOS of Co_2/Si_n ($n = 4$ and 5) without spin polarization.

weak interlayer interaction. In addition, the electron density between A-B bilayer is much denser in hcp Si_4 than in hcp Si_5 [Fig. 6(b)]. The observation that the internal distance d_1 of the surface bilayer [blue balls in Fig. 7(b)] oscillates with the parity of n, being smaller when n is even, also reflecting the sensitivity of the interlayer coupling strength to n. The smaller the spacing, the stronger the interlayer interaction.

One intrinsic factor in deciding the band structure of the heterostructure of hcp Co_2/Si_n is the work function (WF) of the two components, which determines the direction and magnitude of electron transfer when forming the interface [34]. Since the hcp Si_n slab is metallic the WF can be described as $\mathrm{WF} = E_0 - E_f$, where E_0 is the electrostatic potential of a vacuum nearby the surface of the slab. Here, we set the position of E_0 as the bottom plane of the supercell. For hcp Si_9, the calculated WF is 0.319 Ry, which is the same as that obtained with a shorter supercell (the distance between the bottom surface of the slab and the bottom plane of the supercell is 25 Å), indicating that the WF calculated using the original supercell is stable for each slab. As expected, the WF of hcp Si_n exhibits odd-even oscillation behavior with n Fig. 7(b)], and the oscillation phase is equal to that of d_1, which can be well understood in terms of the relationship between WF and the free-electron density around E_f [35]. In short, when n is even, compared with the case when n is odd, the interlayer coupling is stronger and more electrons participate in chemical bonding, so the density of free electrons is relatively small, causing smaller WF.

Combining hcp Si_n with hcp Co_2, one gets an hcp Co_2/Si_n heterostructure in which the $ABAB$ stacking is reserved. Each hcp Co_2/Si_n model system exhibits a negative formation energy [Fig. 7(c)], $\Delta E = E(Co_2/Si_n) - E(Si_n) - E(Co_2)$, indicating the stability of the multilayered structure. With joint Co_2 and Si_n, the chemical potentials of the two tend to be the same, and the relatively large WF of Co_2 (0.374 Ry) causes electrons to move from the Si side to the Co side. Take hcp Co_2/Si_4 as an example. The situation is similar in other systems. The left panel of Fig. 8(a) shows the distribution of electron-density difference of hcp Co_2/Si_4, as $\Delta\rho = \rho(Co_2/Si_4) - \rho(Co_2) - \rho(Si_4)$, in the xz plane before and after the interface formation, and the right panel shows the statistical results along the z axis. A positive value indicates that the electron density increases after the reconstruction of electrons. The most dramatic changes in electron density happen at the Co site, where the electron density increases along the Co-Si direction while decreasing perpendicular to it, demonstrating the interface bonding. The modifications of electrons on Si sites are relatively indistinct but expand towards the inner Si atomic layers with a damped oscillatory behavior. This observation evidences the charge redistribution during the formation of the Co-Si interface.

A question arises whether the interface is stronger when n is odd or when n is even. As mentioned above, the WF of Si_n is larger when n is odd and is closer to that of Co_2, implying more electrons transfer from Si to Co side when forming the interface compared with the case of an even n. We calculated the difference in Co-3d electrons Δn_{3d} between isolated hcp Co_2 and hcp Co_2/Si_n [Fig. 7(d)]. Obviously, the formation of the Co-Si interface increases the occupation numbers of Co-3d states, which oscillate with the parity of n and are in the same phase as WF of hcp Si_n. Therefore, the interface coupling is stronger when n is odd. The calculated

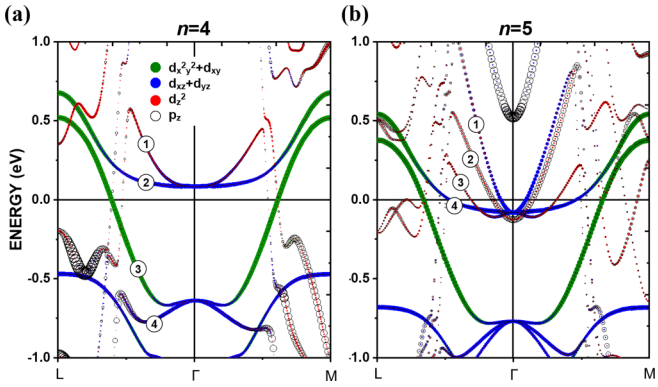

FIG. 9. Band structure with details for Co_2Si_4 (a) and Co_2Si_5 (b). Green, blue, and red circles represent distribution of $d_{x^2y^2}+d_{xy}$, $d_{xz}+d_{yz}$, and d_{z^2} on belt, respectively. Open circles represent distribution of p_z. Size of circle means how much it is occupied, where p orbit is enlarged by 4 times compared to d orbit. Bands ① ② ③ ④ are four bands closest to E_f.

gradient of the work function, as $[\mathrm{WF}(\mathrm{Co_2}) - \mathrm{WF}(\mathrm{Si}_n)]/L$ [the electron redistribution interval, the red arrows shown in Fig. 8(a), further proves this]. For example, when $n = 4$ ($n = 5$), the redistribution interval of the electrons is 5.50 a.u. (5.32 a.u.) and the gradient of the work function is 1.12×10^{-2} Ry/a.u. (0.96×10^{-2} Ry/a.u.). The smaller the work-function gradient, the stronger the interface bonding [36]. So, the Co-Si interface bonding is stronger for the $n = 5$ case. This picture explains the oscillations of the lattice parameters of hcp Co_2/Si_n because the mutual attraction between Co and Si layers leads to a reduction of interlayer distance for a nonpolar lattice, and a stronger interaction resulting in a smaller $d_{\mathrm{Co-Si}}$ and a larger $d_{\mathrm{Co-Co}}$ [Fig. 2(b)]. The *A*-*B* bilayer-like structure also forms in hcp Co_2/Si_n, which is allowed in terms of lattice symmetry since hcp Co_2/Si_n is essentially an hcp-type heterostructure, just like hcp Si_n, except that the electrons are bound by surface potentials in hcp Si_n and by interfacial potentials in hcp Co_2/Si_n.

The band structures provide more information about interface bonding. Let us focus on the four bands around E_f labeled as band ① to band ④ in descending order of energy in Fig. 9. When $n = 4$ [Fig. 9(a)], the $d_{x^2y^2} + d_{xy}$ electrons distribute between Γ and L (M) points for band ② and band ③, the distribution of $d_{xz} + d_{yz}$ and d_{z^2} electrons centered around the Γ point for band ① and band ②. Among them, the contribution of d_{z^2} is the least. The contribution from p_z electrons is negligible for the four bands, indicating weak *p*-*d* interaction. When n is odd, take $n = 5$ as an example [Fig. 9(b)], the four bands intersect near the Γ point, corresponding to the density peak at −0.1 eV in the DOS diagram (Fig. 4). The $d_{x^2y^2} + d_{xy}$ electrons distribute near the L and M points in band ④. The $d_{xz} + d_{yz}$ electrons mainly contribute to band ① and band ④ centered around the Γ point. The d_{z^2} electrons contribute to all of the four bands but are weak. Significantly, band ② has contributions from Si-p_z electrons, a distinct character of *p*-*d* interaction. Accordingly, the interface interaction mainly ascribes to d_{z^2} and p_z electrons in hcp Co_2/Si_5.

As mentioned above, the electron structure of hcp Co_2/Si_n in the vicinity of E_f falls into two categories concerning the parity of n, which is a natural result of the interface effect. We calculated the difference in DOS before and after the formation of hcp Co_2/Si_n[$\Delta\mathrm{DOS} = \mathrm{DOS}(\mathrm{Co_2}/\mathrm{Si}_n) - \mathrm{DOS}(\mathrm{Co_2}) - \mathrm{DOS}(\mathrm{Si}_n)$]. Taking $n = 4$ and $n = 5$ systems as examples, the ΔDOSs of the two systems are similar below −3.0 eV [Fig. 8(b)], indicating that the influence of n mainly affects the valence electrons near E_f. In particular, between −1.0 eV to E_f, although the 3*p*-ΔDOSs of both systems are negative [blue lines in Fig. 8(b)], ascribing to the transport of electrons from Si_n to Co_2 when forming the Co-Si interface, which confirms the above analysis, the curve sinks more for hcp Co_2/Si_5, indicating more Si-3*p* electrons were transferred to the Co_2 side. As a result, the Co-3*d* state accepts fewer electrons from Si for hcp Co_2/Si_4, and the Fermi level happens to cross a Co-3*d* state peak, while for hcp Co_2/Si_5 the Fermi level moves towards the high-energy side due to more extra electrons [Fig. 8(c)]. These observations imply that it seems reasonable to describe the band structure of hcp Co_2/Si_n using a rigid-band model [37].

The oscillation in exchange coupling associated with the parity of n is related to the electronic structure near E_f for hcp Co_2/Si_n. For materials with itinerant magnetism, the FM state is stable when the Fermi level crosses the peak position of the DOS under paramagnetic conditions. Otherwise, the AFM state may take advantage [38]. According to our calculations [Fig. 8(c)], the Fermi level is located at the peak position of DOS in the case of an even number of n, indicating FM ground state, while it just passes the peak when n is an odd number, favoring AFM ground state. When turning on exchange splitting, the spin-majority state moves towards the lower-energy side and the spin-minority state towards the higher-energy side (Fig. 4). For systems with even n, the state with center originally at E_f moves above it and E_f passes through the foot of the Co-3*d* density state, while for systems with odd n, the state originally under E_f now happens to move its center to E_f.

The oscillation of the magnetic-moment SMM with n in hcp Co_2/Si_n can be understood by exploring the spin-resolved details of the charge transfer during the formation of the interface bonding. According to our calculations, the redistribution of spin-minority states dominates ΔDOS [orange shadow areas in Fig. 8(b)] in the range from −2.5 eV to E_f and higher energy, while in the energy region below −2.5 eV, ΔDOS is mainly determined by the spin-majority states [blue shadow areas in Fig. 8(b)]. Considering that the center of the Si-*p*(z) state of Si_n is above −2.0 eV, the minority state of the 3*d* electron plays a leading role in constructing the Co-Si interface. This is proved by the opposite sign of the spin moment of Si and Co atoms in hcp Co_2/Si_n. By integrating ΔDOS from $-6.0\ \mathrm{eV} \sim E_f$, it is found that the difference in occupation number of spin-up Co-3*d* electrons, $\Delta\rho\uparrow$, is −1.084 when $n = 5$ and −1.00 when $n = 4$, which are similar. But, the differences in occupation number of spin-down electrons are distinct, i.e., $\Delta\rho\downarrow$, is −0.278 when $n = 5$ and −1.021 when $n = 4$. Since the variation in Co moment after forming the Co-Si interface is $\mathrm{SMM} = \Delta\rho\uparrow - \Delta\rho\downarrow$, SMM is more reduced when $n = 5$, inducing oscillatory behavior in the Co moment.

The quantum oscillation of OMM is related to the *n*-dependent lattice symmetry. In 3*d*–transition-metal compounds, the orbital angular momenta are totally or partially

quenched by the crystal field and/or the hybridization effects, resulting in a small OMM. Generally, the higher the symmetry of the local environment of the atom, the more thorough the quenching will be [26]. As discussed above, when n is odd, compared with the case when n is even, the lattice symmetry of the supercell is high, which prejudices orbital quenching of d electrons hence reducing OMM.

The oscillation of ΔE_{SOC} comes from the combination of SMM and OMM. The SOC interaction is defined as $H_{so} = \lambda \sum_i \hat{l}_i \cdot \hat{s}_i$, where $\hat{l}_i$ and $\hat{s}_i$ are the one-electron orbital and spin operators, respectively, and the sum runs over all electrons. For the present case, the SOC-induced band gap at the Γ point can be simplified as $\Delta E_{\mathrm{SOC}} \sim [+m_{\mathrm{j}}\mu_{\mathrm{eff}} - (-m_{\mathrm{j}}\mu_{\mathrm{eff}})] = 2|m_{\mathrm{j}}|\mu_{\mathrm{eff}}$, where μ_{eff} is proportional to the SMM of the Co atom, and m_j is the magnetic quantum number of the unquenched $3d$ orbital, which represents the effective magnetic field caused by the SOC effect and is proportional to the OMM of the Co atom. Since SMM and OMM have the same oscillation tendency with n, the oscillation of ΔE_{SOC} splitting with n should be synchronized.

Essentially, the odd-even quantum oscillations observed in the hcp Co_2/Si_n superlattice arise from the interlayer interactions, which are sensitive to the lattice symmetry. The interlayer coupling strength is modulated through the combined action of the A-B bilayer stacking periodicity of the hcp lattice and the surface or interface potential. When the A-B bilayer period is complete for Si_n, i.e., when n is even, the work function departs from that of Co_2 due to the stronger inner coupling of Si_n surface bilayers, which causes weak interface bonding in hcp Co_2/Si_n. Thus, the interface strength varies with the parity of n, resulting in quantum oscillations of related properties, such as lattice parameters, work functions, electronic structures near E_f, and magnetic properties. Our study shows that it is feasible to adjust the lattice symmetry, hence interlayer coupling, by adjusting the stacking of atomic layers, such as the atomic arrangement and chemical composition of a single layer and the number and sequence of stacking layers, for an hcp-structured multilayer. The rapid development of the latest technology provides the possibility for practical application.

IV. CONCLUSIONS

We performed a detailed first-principles study of the quantum oscillations in hcp Co_2/Si_n superlattices, including lattice parameters, electronic structures around the Fermi energy, exchange coupling, magnetic moment, and SOC-induced band splitting. The observed odd-even oscillations result from the A-B bilayer period characteristic of the hcp structure, which makes the lattice symmetry dependent on the parity of n. When the period is complete, Si_n and Co_2 form a weak interface. The modulation of the interface strength by Si_n causes other properties to oscillate with n. Our study proposes a feasible method to tune the electromagnetic properties of materials from the perspective of crystal symmetry and provides an idea for developing metal-semiconductor heterojunctions.

ACKNOWLEDGMENTS

The authors are grateful for support from the National Natural Science Foundation of China under Grant No. 11975007. The authors are thankful for the technical and hardware support provided by the Lanzhou University Supercomputing Center [39].

[1] I. B. Altfeder, J. A. Golovchenko, and V. Narayanamurti, Confinement-Enhanced Electron Transport across a Metal-Semiconductor Interface, Phys. Rev. Lett. **87**, 056801 (2001).

[2] D. Vashaee and A. Shakouri, Improved Thermoelectric Power Factor in Metal-Based Superlattices, Phys. Rev. Lett. **92**, 106103 (2004).

[3] B. Biswas, S. Nayak, V. Bhatia, A. I. K. Pillai, M. Garbrecht, M. H. Modi, M. Gupta, and B. Saha, Interfacial chemistry and electronic structure of epitaxial lattice-matched $TiN/Al_{0.72}Sc_{0.28}N$ metal/semiconductor superlattices determined with soft x-ray scattering, J. Vac. Sci. Technol. A **38**, 053201 (2020).

[4] A. Majumdar and P. Reddy, Role of electron–phonon coupling in thermal conductance of metal-nonmetal interfaces, Appl. Phys. Lett. **84**, 4768 (2004).

[5] J. Tan, S. Li, B. Liu, and H.-M. Cheng, Structure, preparation, and applications of 2D material-based metal-semiconductor heterostructures, Small Structures **2**, 2000093 (2020).

[6] A. Ziane, S. Bouarab, C. Demangeat, and A. Vega, Interfacial effects on the magnetic profiles and interlayer exchange coupling of Co/CoSi multilayers, Thin Solid Films **520**, 302 (2011).

[7] P. Vlaic, E. Burzo, and K. Carva, Oscillatory exchange coupling and strong direct tunnelling with AgCl based heterojunctions, J. Alloys Compd. **630**, 299 (2015).

[8] A. A. Kistanov, Y. Cai, K. Zhou, N. Srikanth, S. V. Dmitriev, and Y. W. Zhang, Exploring the charge localization and band gap opening of borophene: A first-principles study, Nanoscale **10**, 1403 (2018).

[9] F. Lavini, A. Calo, Y. Gao, E. Albisetti, T. D. Li, T. Cao, G. Li, L. Cao, C. Aruta, and E. Riedo, Friction and work function oscillatory behavior for an even and odd number of layers in polycrystalline MoS_2, Nanoscale **10**, 8304 (2018).

[10] T. L. Chan, C. Z. Wang, M. Hupalo, M. C. Tringides, and K. M. Ho, Quantum Size Effect on the Diffusion Barriers and Growth Morphology of Pb/Si(111), Phys. Rev. Lett. **96**, 226102 (2006).

[11] X. J. Liu, C. Z. Wang, M. Hupalo, H. Q. Lin, K. M. Ho, and M. C. Tringides, Quantum confinement induced oscillatory electric field on a stepped Pb(111) film and its influence on surface reactivity, Phys. Rev. B **89**, 041401(R) (2014).

[12] J. Enkovaara, A. Ayuela, and R. M. Nieminen, Interlayer coupling in Co/Si sandwich structures, Phys. Rev. B **62**, 16018 (2000).

[13] N. Yaacoub, C. Meny, O. Bengone, and P. Panissod, Short Period Magnetic Coupling Oscillations in Co/Si Multilayers: Theory versus Experiment, Phys. Rev. Lett. **97**, 257206 (2006).

[14] H. Sevincli, R. T. Senger, E. Durgun, and S. Ciraci, Oscillatory exchange coupling in magnetic molecules, J. Phys.: Condens. Matter **19**, 216205 (2007).

[15] J. Tong, L. Ruan, X. Yao, F. Tian, G. Qin, and X. Zhang, Unexpected magnetic coupling oscillations for $L1_0$–MnGa/Co(Fe) films induced by quantum wells, Phys. Rev. B **97**, 184426 (2018).

[16] Y. E. Suyolcu, G. Christiani, P. A. van Aken, and G. Logvenov, Design of complex oxide interfaces by oxide molecular beam epitaxy, J. Supercond. Nov. Magn. **33**, 107 (2019).

[17] Y.-H. Zhang and D. J. Smith, Heterovalent semiconductor structures and devices grown by molecular beam epitaxy, J. Vac. Sci. Technol. A **39**, 030803 (2021).

[18] D. Jung, J. Norman, Y. Wan, S. Liu, R. Herrick, J. Selvidge, K. Mukherjee, A. C. Gossard, and J. E. Bowers, Recent advances in InAs quantum dot lasers grown on on-axis (001) silicon by molecular beam epitaxy, Phys. Status Solidi A **216**, 1800602 (2018).

[19] P. Aseev, A. Fursina, F. Boekhout, F. Krizek, J. E. Sestoft, F. Borsoi, S. Heedt, G. Wang, L. Binci, S. Marti-Sanchez *et al.*, Selectivity map for molecular beam epitaxy of advanced III-V quantum nanowire networks, Nano Lett. **19**, 218 (2019).

[20] R. Ahuja, O. Eriksson, and B. Johansson, Theoretical high-pressure studies of silicon VI, Phys. Rev. B **60**, 14475 (1999).

[21] T. M. Manhabosco and I. L. Müller, Deposition of thin cobalt films onto silicon by galvanostatic and potentiostatic techniques, J. Mater. Sci. **44**, 2931 (2009).

[22] L. A. d. S. Ries, H. A. de Brito, F. P. Gasparin, and I. L. Muller, Additive-free electrodeposition of cobalt on silicon from 1-butyl-3-methylimidazolium tetrafluoroborate ionic liquid, J. Mol. Liq. **325**, 114787 (2021).

[23] B. A. Taylor and R. W. Floyd, Precision measurements of lattice parameters of non-cubic crystals, Acta Crystallogr. **3**, 285 (1950).

[24] G. K. H. Madsen, P. Blaha, K. Schwarz, E. Sjöstedt, and L. Nordström, Efficient linearization of the augmented plane-wave method, Phys. Rev. B **64**, 195134 (2001).

[25] K. Schwarz, P. Blaha, and G. K. H. Madsen, Electronic structure calculations of solids using the WIEN2k package for material sciences, Comput. Phys. Commun. **147**, 71 (2002).

[26] I. G. Rau, S. Baumann, S. Rusponi, F. Donati, S. Stepanow, L. Gragnaniello, J. Dreiser, C. Piamonteze, F. Nolting, S. Gangopadhyay *et al.*, Reaching the magnetic anisotropy limit of a 3D metal atom, Science **344**, 988 (2014).

[27] G. Bihlmayer, Y. M. Koroteev, P. M. Echenique, E. V. Chulkov, and S. Blügel, The Rashba-effect at metallic surfaces, Surf. Sci. **600**, 3888 (2006).

[28] A. Manchon, H. C. Koo, J. Nitta, S. M. Frolov, and R. A. Duine, New perspectives for Rashba spin-orbit coupling, Nat. Mater. **14**, 871 (2015).

[29] S. J. Zhang, W. X. Ji, C. W. Zhang, P. Li, and P. J. Wang, Two-dimensional large gap topological insulators with tunable Rashba spin-orbit coupling in group-iv films, Sci. Rep. **7**, 45923 (2017).

[30] S. J. Duclos, Y. K. Vohra, and A. L. Ruoff, hcp to fcc Transition in Silicon at 78 GPa and Studies to 100 GPa, Phys. Rev. Lett. **58**, 775 (1987).

[31] M. Hanfland, U. Schwarz, K. Syassen, and K. Takemura, Crystal Structure of the High-Pressure Phase Silicon VI, Phys. Rev. Lett. **82**, 1197 (1999).

[32] A. A. Mostofi, J. R. Yates, Y.-S. Lee, I. Souza, D. Vanderbilt, and N. Marzari, wannier90: A tool for obtaining maximally-localised Wannier functions, Comput. Phys. Commun. **178**, 685 (2008).

[33] N. Marzari, A. A. Mostofi, J. R. Yates, I. Souza, and D. Vanderbilt, Maximally localized Wannier functions: Theory and applications, Rev. Mod. Phys. **84**, 1419 (2012).

[34] F. K. Schulte, A theory of thin metal films: Electron density, potentials and work function, Surf. Sci. **55**, 427 (1976).

[35] G. Hua and D. Li, Generic relation between the electron work function and Young's modulus of metals, Appl. Phys. Lett. **99**, 041907 (2011).

[36] D. Y. Li, L. Guo, L. Li, and H. Lu, Electron work function - a probe for interfacial diagnosis, Sci. Rep. **7**, 9673 (2017).

[37] Y. N. Zhang, J. X. Cao, and R. Q. Wu, Rigid band model for prediction of magnetostriction of iron-gallium alloys, Appl. Phys. Lett. **96**, 062508 (2010).

[38] G. Fabricius, A. M. Llois, and H. Dreyssé, Ferromagnetic stability and density of states, Phys. Rev. B **48**, 6665 (1993).

[39] https://hpc.lzu.edu.cn/.